Surface-Induced Polymer Crystallization in High Volume Fraction Aligned Carbon Nanotube–Polymer Composites[a]

Shanju Zhang, Wei Lin, Xinfei Yu, Ching-Ping Wong, Stephen Z. D. Cheng, David G. Bucknall*

Surface-induced crystallization of high-density polyethylene in vertically aligned multiwalled carbon nanotube arrays has been investigated by means of scanning electron microscopy (SEM), wide-angle X-ray diffraction (WAXD), differential scanning calorimetry (DSC) and thermogravimetric analysis (TGA). 1-mm long nanotube arrays are infiltrated by polyethylene solutions and then the system is allowed to crystallize under controlled conditions. Periodic disk-shaped polyethylene single crystals grow perpendicularly to the aligned nanotubes but do not completely fill the intertube spacing, forming oriented 3D porous structures. This unique morphology leads to low density, high nanotube mass fraction (up to 80 wt.-%) composites. Microstructure (WAXD) analysis shows that the nanotubes act as both orientation templates as well as nucleating agents for polyethylene crystallization creating orthorhombic and monoclinic forms, although the overall crystal structure is dominated by the orthorhombic form. Thermal analysis (DSC) shows that the nanocomposite exhibits multiple phase transitions during heating and cooling with a weak superheating and supercooling dependence on different scanning rates. Three phase structures have been identified and a possible model is proposed to explain the observed phenomenon.

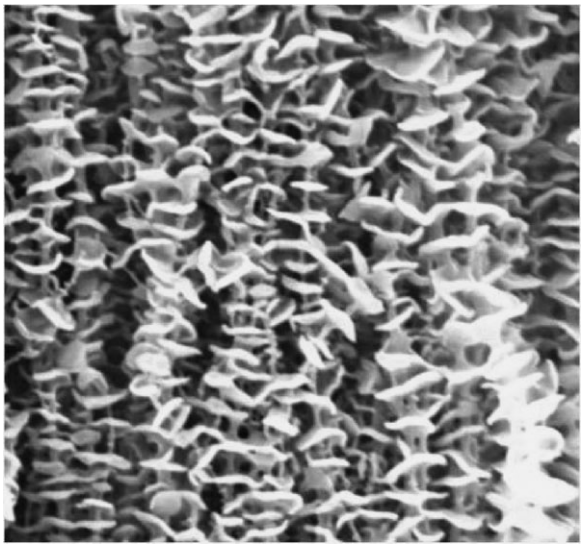

D. G. Bucknall, S. Zhang
School of Polymer, Textile and Fiber Engineering, Georgia Institute of Technology, Atlanta, GA 30332-0295, USA
Fax: +404 894 8780; E-mail: david.bucknall@ptfe.gatech.edu

S. Zhang
Current address: Department of Chemical Engineering, Yale University, New Haven, CT 06511, USA
E-mail: shanju.zhang@yale.edu
W. Lin, C.-P. Wong
School of Materials Science and Engineering, Georgia Institute of Technology, Atlanta, GA 30332-0245, USA
X. Yu, S. Z. D. Cheng
Department of Polymer Science, Maurice Morton Institute, The University of Akron, Akron, Ohio 44325-3909, USA

[a] Supporting information for this article is available at the bottom of the article's abstract page, which can be accessed from the journal's homepage at http://www.mcp-journal.de, or from the author.

DOI: 10.1002/macp.200900686

Introduction

Carbon nanotubes (CNTs) are considered as promising fillers for polymer nanocomposites, as they possess molecular sized dimensions, large aspect ratios, very high strength and stiffness, and excellent electronic and thermal properties.[1–5] Addition of small amounts of CNTs can have a large effect on the thermal and mechanical properties, electrical conductivity, and rheological behavior of polymers.[6–11] However, practical application of these nanocomposites strongly depends on the quality of the CNT-polymer interface. Theoretical simulations and experimental observations have shown that strong interfacial strength can be obtained by introducing chemical or physical bonding between CNTs and polymers.[12–15]

In semicrystalline polymer composites, CNTs can also act as an orientation template and heterogeneous nucleating agent for polymer orientation and crystallization.[16–20] At the CNT surfaces, the polymer forms an ordered crystal layer with molecular chains orienting along the CNT axis. As CNTs have large surface areas, polymer crystallization confined on CNT surfaces will behave differently from those in the bulk, leading to changes in chain mobility, chain conformation, and chain packing. The polymer molecular ordering at the CNT interface is expected to play an important role in enhancing the properties of CNT-polymer composites.[21–23] However, it is challenging to fabricate CNT-polymer composites with a predominant interfacial phase, as processing difficulties limit dispersing high volume fraction CNTs in polymers.

Recent advances in CNT synthesis allow production of millimeter long aligned CNT arrays.[24–27] These ultra long aligned CNT arrays provide an opportunity for fabricating novel polymer nanocomposites with superior properties, since the polymer is reinforced by continuous aligned nanotubes.[28] One distinct advantage for making such novel polymer composites using long CNT arrays is the very large volume between the CNTs into which the polymers can be infiltrated. Monomer liquid or polymer solution can be infiltrated into the CNT arrays, followed by in situ polymerization or solvent evaporation, respectively.[29–32] Consequently, the CNTs are distributed, thereby overcoming the dispersion problems that occur in the bulk nonaligned CNTs composites formed simply by mixing. High CNT volume fraction (up to 20%) polymer composites have been reported based on long CNT arrays where up to 100% of the polymer volume fraction could be interphase.[33,34] However, to the best of our knowledge, there are no reports of polymer crystallization confined in the long CNT arrays to date. In this work, we report polyethylene crystallization in 1-mm long CNT-array based composites with a CNT loading up to 80 wt.-%.

Experimental Part

The CNT arrays were synthesized in our laboratory by chemical vapor deposition (CVD).[35,36] The CNTs produced were multiwalled with an average diameter of 10 nm and length of 1.0 mm. The density of CNTs in arrays was estimated about 1 500 μm^{-2}.[36] The as-grown CNT arrays were soaked in a solution of high-density polyethylene (HDPE, MFI = 12 g/10 min, Aldrich Co.) in *p*-xylene at 120 °C for 10 min. The polymer solution concentration was varied from 0.05 to 5.0 wt.-%. The solution was then placed in an oil bath with a preset temperature at 104 °C to allow crystallization. After crystallization, the CNT arrays were taken out of solution and rinsed with ethanol. The samples were dried at 50 °C under vacuum overnight before further characterization was performed. Isothermal crystallization kinetics for one system was conducted at 104 °C using a solution concentration of 1 wt.-%. Samples were removed from the solution at different crystallization times, and after rinsing and drying using the method described above, were characterized by SEM.

Scanning electron microscopy (SEM) images of gold-coated samples were obtained with a LEO-1 530 microscope operated at an accelerating voltage of 5 kV. WAXD data were collected with a Rigaku 18 kW rotating anode X-ray generator attached to an R-AXIS-IV image plate system. Calibration was performed using silicon powder in the high-angle region (>15°) and silver behenate in the low-angle region (<15°). Background scattering was subtracted from the sample patterns. A hot stage with temperature control of ±0.5 °C was used to obtain diffraction patterns at elevated temperatures. The exposure time for each WAXD pattern was 15 min. Thermal properties were measured using a differential scanning calorimetry (DSC Q-200, TA Instruments) with a scanning rate of 10 °C · min^{-1} under nitrogen. Thermogravimetric analysis (TGA) was performed using a TGA-Q5000 (TA Instruments) with a heating rate of 10 °C · min^{-1} under nitrogen.

Results and Discussion

Figure 1 shows SEM images of the morphology of composites prepared at different solution concentrations of PE in xylene after 12 h of crystallization. At a low solution concentration of 0.05 wt.-% (Figure 1a), the aligned CNTs are periodically decorated by disk-shaped PE single crystals, leading to an oriented hybrid shish-kebab nanostructure.[37–39] The average lateral dimension of PE crystals is ≈70 ± 30 nm and the average periodicity is ≈40 ± 20 nm. CNT-induced hybrid shish-kebab nanostructures were first reported by Li et al. in PE solution crystallization.[39] Such hybrid nanostructures have also been found in nylon, poly(vinyl alcohol) (PVA), poly(ethylene glycol) (PEG), and polyethylene-*block*-poly(ethylene oxide) (PE-*b*-PEO).[38,40,41] It is believed that the hybrid nanostructures occur due to geometric confinement, wherein no strict lattice matching occurs but cooperative orientation of polymer chains and the CNT axis is required.[38] Although PE crystals can also bind several CNTs together forming a multi-shish core,[42] we observed that PE crystals growing from adjacent aligned

Macromol. Chem. Phys. **2010**, *211*, 1003–1011

Macromolecular Journals

DOI: 10.1002/macp.200900686

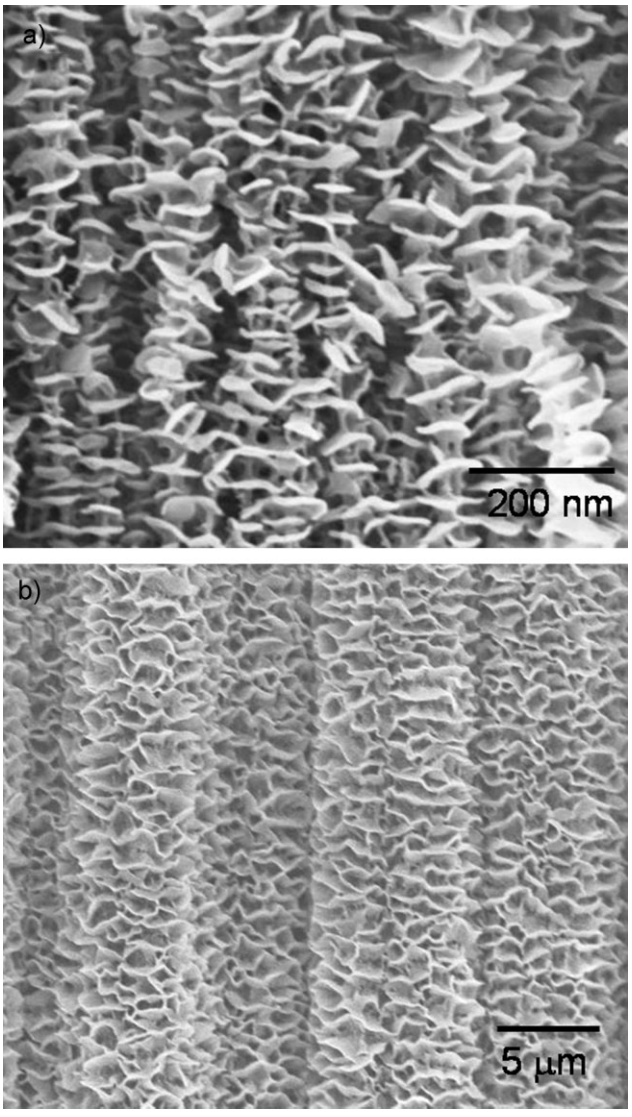

Figure 1. Electron micrographs of surface structures of the nanotube-polyethylene composites prepared from different solution concentrations after 12 h of crystallization. (a) 0.05 wt.-% and (b) 2.0 wt.-%.

CNTs interpenetrated with each other (Figure 1a). In these CNT arrays the geometry confines the PE crystals to grow perpendicularly to the CNT axis and therefore the PE chains are parallel to this axis. Importantly, the interpenetration of oriented PE crystals results in an interlocking effect,[43,44] which physically lock the aligned CNTs together and enhance load transfer from the PE crystals to the individual CNTs when the sample is stretched. By contrast samples prepared in a solution concentration of 2 wt.-% produce systems where the CNT arrays are covered by extensive PE crystal growth, so much so that the individual CNTs can no longer be identified (Figure 1b). The crystal size of PE from 2 wt.-% solution is significantly larger than that from 0.05 wt.-% solution, with diameters of several microns.

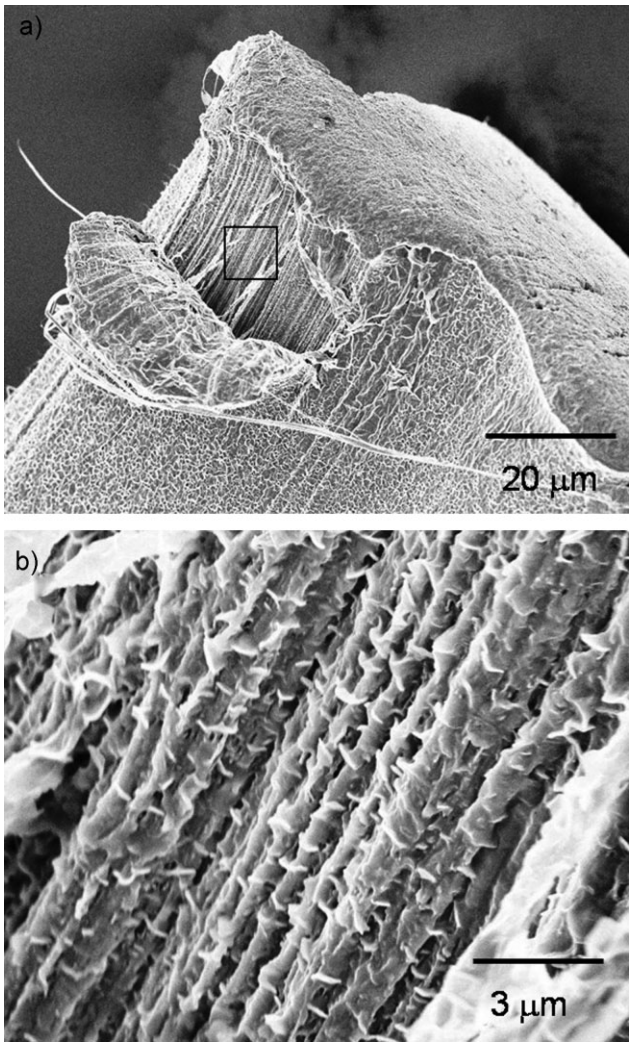

Figure 2. Electron micrographs of the internal structure of the composite prepared from 1.0 wt.-% solution after 12 h of crystallization. (a) overall structure and (b) large magnification of the square area in (a).

To ensure that the PE crystals have grown throughout the bulk of the CNT arrays, the skin of the nanocomposite was peeled off to reveal the internal morphology (Figure 2a). Hybrid shish-kebab nanostructures were clearly observed within the internal volume of the CNT array (Figure 2b), although PE crystals on the skin are much larger than those inside the CNT array. It is assumed that the small size of PE crystals inside the CNT array is due to the limited growth under geometric confinement. Despite the growth of PE crystals as observed on the external surface of the sample, the diameter and therefore the degree of interlocking of the supramolecular structures are considerably reduced. This effect may ultimately affect the mechanical properties of resultant nanocomposites.

By changing solution concentrations, we are able to control the CNT loading in the composites using TGA to

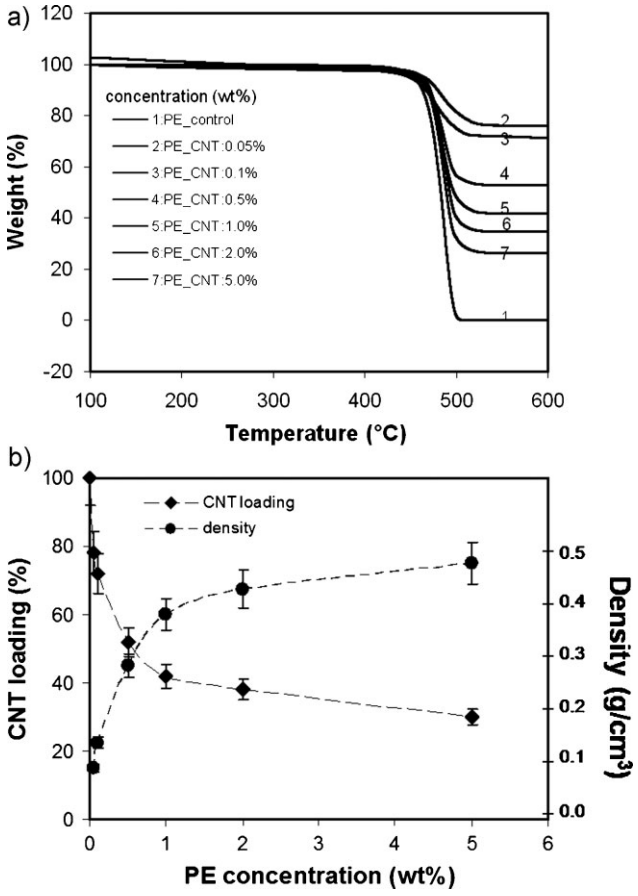

Figure 3. (a) TGA plots of the composites prepared from different solution concentrations shown in the figure and (b) nanotube loading and composite density dependence on the polymer concentration crystallized at 104 °C for 12 h. The dash lines are drawn to guide the eye only.

measure the weight loss of the composites. Figure 3a shows the TGA plots of the composites prepared by different solution concentrations. The weight fractions of nanotubes in the composites were determined to be 30–80 wt.-%, depending on the initial solution conditions. To the best of our knowledge, such ultrahigh loadings of long CNTs in polymer composites have not been achieved by existing processing technologies. Contrary to current strategies for fabricating CNT-polymer composites, the intertube spacing in our long CNT-polymer composites is not totally filled with polymer crystals.

The effect of PE solution concentration on CNT loading and composite density is shown in Figure 3b. At the solution concentrations below 1 wt.-%, the CNT loading in the composite decreased rapidly with increasing concentration. Increase in the solution concentration above 1 wt.-% results in a less dramatic decrease in CNT loading. This observation suggests that the PE crystal growth may slow down inside the CNT array and increase in solution concentration only results in the PE crystal growth on the surface of the CNT array. For concentrations above 1 wt.-%, this leads to the composite density increasing monotonically with solution concentration.

PE crystallization kinetics on the aligned CNTs was studied further using a solution concentration of 1 wt.-% annealed at 104 °C. SEM imaging shows that the crystal dimensions vary less than 10% in dimension, clearly indicating that the polymer crystals grow homogeneously across the whole of the sample. Figure 4 shows the growth of PE crystals on the CNTs as a function of crystallization time. A simple linear slope of $\approx 25\,\mathrm{nm \cdot h^{-1}}$ indicates a constant crystal growth rate, which is consistent with a heterogeneous nucleation growth mechanism.[45] Recently, polypropylene trans-crystallization kinetics on the CNTs was reported and the heterogeneous nucleation growth was also identified.[21]

A typical 2-D WAXD pattern of the CNT-PE composite and its corresponding radically averaged 1-D plot are shown in Figure 5. Anisotropy in the 2-D WAXD pattern was observed (see Figure 5a), which is associated with the oriented PE crystals and CNTs. The reflection at $2\theta = 25.5^\circ$ corresponds to the graphite (002) plane of the CNTs.[46] The main peaks located at $2\theta = 21.5^\circ$ and 23.9° are the (110) and (200) reflections of orthorhombic PE, respectively (see Figure 5b).[47] Both $(110)^O$ and $(200)^O$ reflections are in the equatorial plane, indicating non-twisted PE crystals without an *a*-axis orientation. Detailed analysis shows that there is an additional reflection located at $2\theta = 19.5^\circ$, unique to the (010) monoclinic form of PE.[47] The presence of monoclinic crystals in ultrahigh weight ratio long CNT-PE composites is very interesting, since the monoclinic phase in PE is shown to be metastable and is generally only obtained under either high pressure[48,49] or high

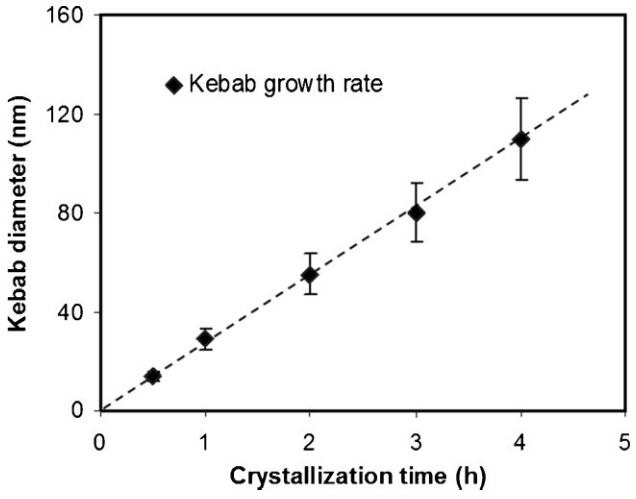

Figure 4. Polymer kebab crystal diameter dependence on the crystallization time for the composite prepared from 1.0 wt.-% solution at 104 °C. The dash line is drawn to guide the eye only.

Macromol. Chem. Phys. **2010**, *211*, 1003–1011

Macromolecular Journals
DOI: 10.1002/macp.200900686

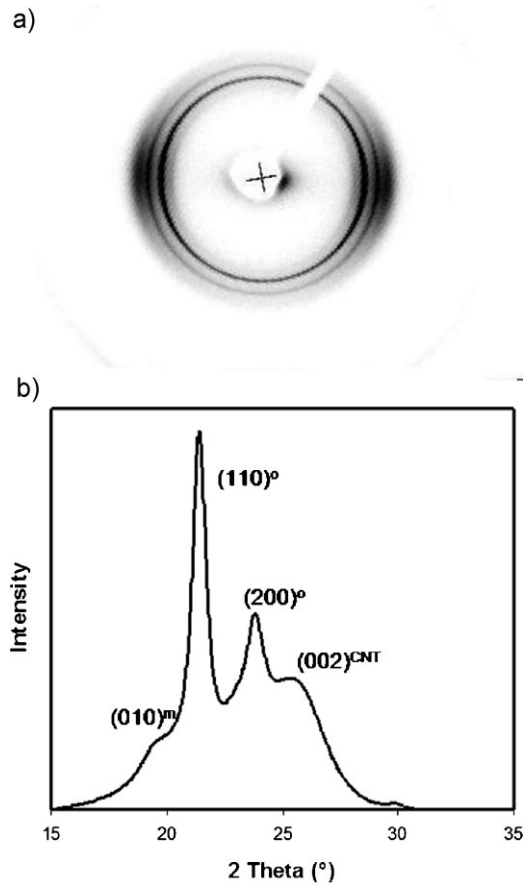

Figure 5. Wide-angle X-ray diffractions of the composites prepared from 1.0 wt.-% solution for 0.5 h of crystallization. (a) 2-D WAXD pattern and (b) integrated radial scan of (a).

deformation, for example during mechanical stretching.[50,51]

Azimuthal intensity scans of the 2D data for the $(002)^{CNT}$, $(110)^{O}$, and $(010)^{M}$ reflections in Figure 5a are shown in Figure 6. The values of full width at half-maximum (FWHM) for the $(002)^{CNT}$, $(110)^{O}$, and $(010)^{M}$ curves are 41.5°, 47.8° and 45.5°, respectively. Consequently, the maximum degree of misalignment of the CNTs and the polymer chains in orthorhombic and monoclinic forms are ±20.8°, ±23.9°, and ±22.8°, respectively. The data also show that the PE crystals are oriented in the same direction to that of the CNTs. These results indicate that CNTs act as an orientation template for PE crystallization in both orthorhombic and monoclinic forms.

The crystal sizes of both the orthorhombic $(100)^{O}$ and monoclinic $(010)^{M}$ forms in the composites as functions of concentration and crystallization time were determined using the Scherrer equation ($\tau = K\lambda/(\beta \cdot \cos\theta)$, where τ is the average crystal size, K the shape factor set to be 0.9, λ the wavelength, β the value of FWHM, and θ is the Bragg angle).

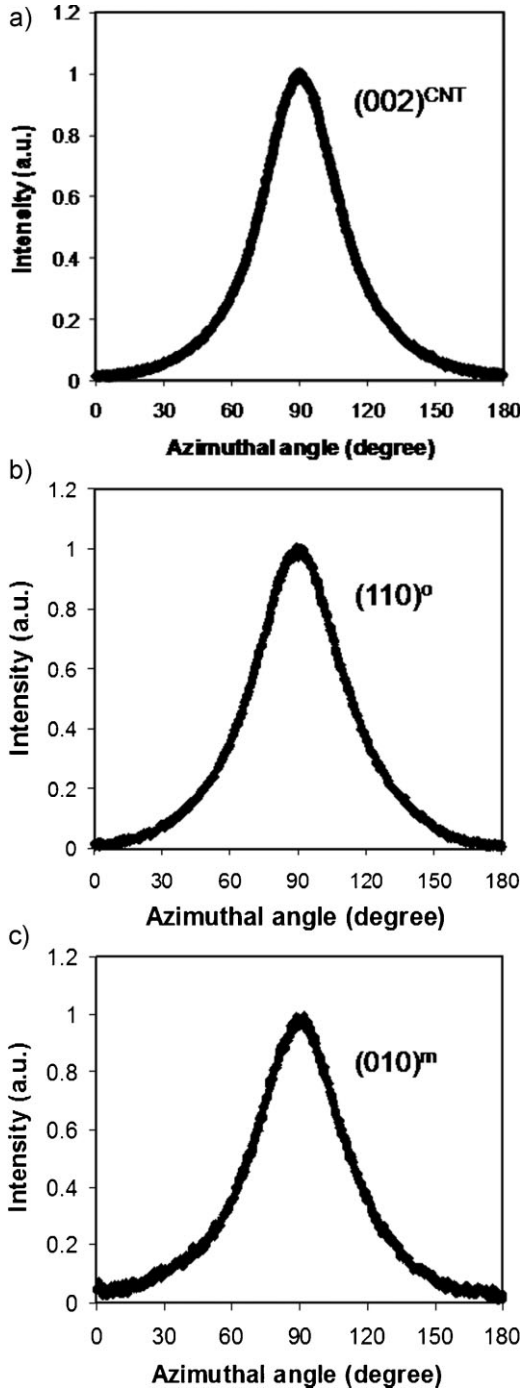

Figure 6. Azimuthal intensity scans of the 2-D data in Figure 5a. (a) (002) reflection for CNTs, (b) (110) reflection for PE orthorhombic form, and (c) (010) reflection for PE monoclinic form.

For samples all annealed for 12 h at 104 °C, and using this equation a clear dependence of the crystal size on the solution concentration is observed (Figure 7a). For solution concentrations below 1 wt.-%, the crystal sizes of both orthorhombic and monoclinic forms increase rapidly with

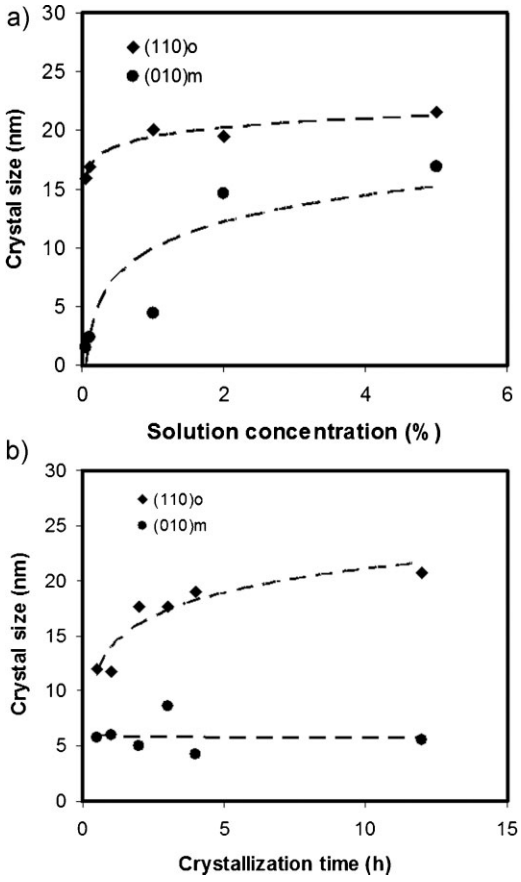

Figure 7. Crystal sizes of (110)o and (010)m planes dependence on (a) solution concentration for 12 h of crystallization and (b) crystallization time from 1 wt.-% solution. In the plots, the dash lines are drawn to guide the eye only.

increasing concentration. This observation indicates that the CNTs act as a nucleating agent for both orthorhombic and monoclinic forms. The crystal size of the monoclinic form is significantly smaller than that of the orthorhombic, since the monoclinic crystals grow much faster than the orthorhombic.[52] For increasing concentrations above 1 wt.-%, a slight increase in the crystal sizes of both orthorhombic and monoclinic forms was observed. The effect of crystallization time on crystal size was also investigated for the composite prepared using a 1 wt.-% solution (see Figure 7b). With an increase of crystallization time, the crystal size of the orthorhombic form increases monotonically. By contrast the monoclinic crystals form very rapidly and then their size remains effectively independent of crystallization time.

Figure 8 shows heating and cooling DSC thermograms of the CNT-PE composite prepared from a 1 wt.-% solution after 12 h of crystallization, from which multiple melting and crystallization behaviors can be observed. The main endothermic peak $T_{m1} \approx 124.5\,^{\circ}C$ from the 1st and 2nd heating curves can be clearly identified, corresponding to

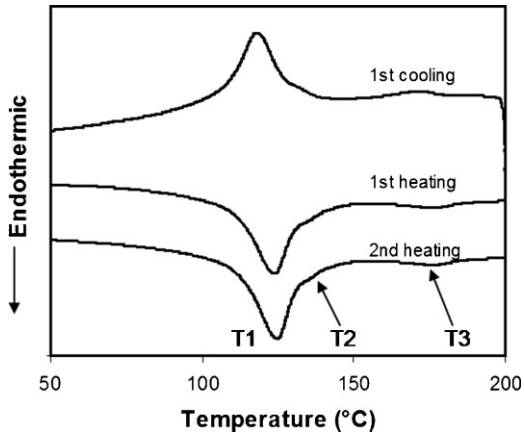

Figure 8. DSC curves of the composite prepared from 1 wt.-% solution for 12 h of crystallization during the first heating, first cooling and second heating processes. The arrows show the high temperature peaks.

the orthorhombic phase of the control PE, i.e., pure PE ($T_m \approx 126.7\,^{\circ}C$). The slight reduction in the melting point in the nanocomposites, compared to the pure PE, is attributed to the small size imperfect polymer crystals induced by CNTs. In addition to the obvious orthorhombic melting peak, there are two further weak endothermic peaks at $T_{m2} \approx 135.5\,^{\circ}C$ and $T_{m3} \approx 175.5\,^{\circ}C$. These peaks are associated with phases that do not exist in the pure PE and are related to polymer chain conformations at the interfacial phase at the CNT surfaces (as discussed below). It should be noted that the monoclinic phase of PE, which should melt around 80 °C, was not detectable by DSC, which is consistent with the literature.[47] The reversibility of the phase behavior is evidenced by the presence of the corresponding exothermic peaks in the cooling curve with three exothermic peaks at $T_{c3} \approx 172.5\,^{\circ}C$, $T_{c2} \approx 130.5\,^{\circ}C$, and $T_{c1} \approx 117.7\,^{\circ}C$, respectively.

To get more insight into the physical origin of the higher temperature peaks, further DSC measurements at different scanning rates were undertaken for this sample. Figure 9 shows a series of DSC heating and cooling curves obtained at different scanning rates. For all the scanning rates, three phase transitions were observed. In addition, these transition temperatures are largely unaffected by superheating and supercooling (see Figure 10), in complete contrast to the behavior of pure PE.[53] Extrapolating these data to zero heating rates results in melting temperatures of $T_{m1} \approx 123.8$, $T_{m2} \approx 134.6$, and $T_{m3} \approx 175.1\,^{\circ}C$, while extrapolating to zero cooling rates leads to crystallization temperatures of $T_{c1} \approx 119.0$, $T_{c2} \approx 133.5$, and $T_{c3} \approx 172.7\,^{\circ}C$. These observations demonstrate that CNT surface provide extensive nucleation sites for polymer crystal growth.

Figure 11 shows the WAXD patterns at different temperatures obtained during heating of the sample. As the WAXD patterns during cooling are almost identical to

Macromol. Chem. Phys. **2010**, *211*, 1003–1011

Macromolecular Journals
DOI: 10.1002/macp.200900686

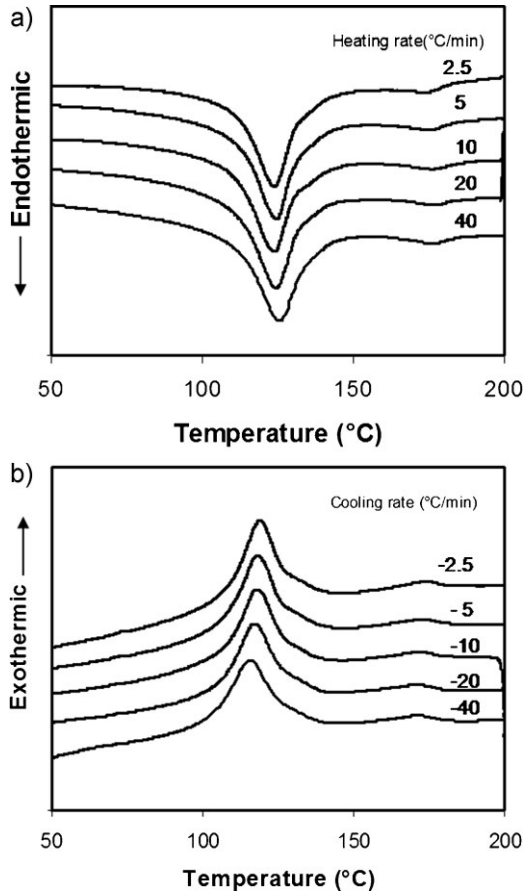

Figure 9. DSC heating and cooling curves at different scanning rates for the same samples in Figure 8.

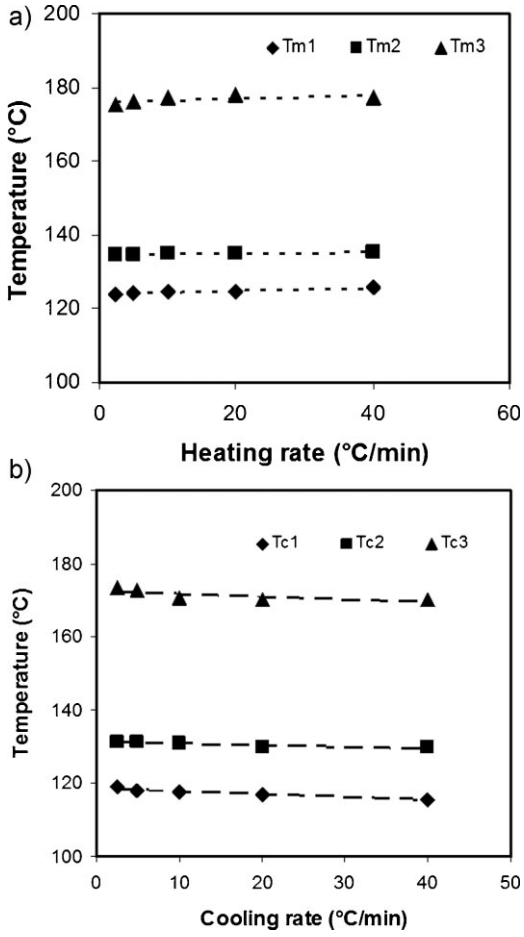

Figure 10. Plots of phase transition temperatures against scanning rates. (a) Heating and (b) cooling. The dash lines are drawn to guide the eye only.

those during heating, only the WAXD heating data are discussed here. These observations demonstrate that phase transitions are thermodynamically reversible. Based on the room-temperature structural analysis, both orthorhombic and monoclinic forms of PE crystals are identified. During heating, the intensity of the monoclinic (010) reflection decreases while the intensities of orthorhombic (110) and (200) reflections increase. This phenomenon indicates that the monoclinic form is gradually transformed into the orthorhombic form. Loss of the monoclinic (010) reflection at 80 °C shows that the transformation from the monoclinic to the orthorhombic form is completed at this temperature.[54,55] During heating the peak positions of the orthorhombic (110) and (200) reflections shift slightly toward lower 2θ angles, indicating an increase in *d*-spacings, which is attributed to the thermal expansion during heating.

When the temperature reaches 125 °C, the intensities of the orthorhombic (110) and (200) reflections suddenly decrease and an amorphous scattering halo appears. Weak orthorhombic reflections persist until heated above 135 °C. These data together with those from DSC indicate that the PE crystals in the bulk melt to a liquid state at 125 °C, but the PE crystals at the CNT interface do not melt at this temperature and are still in an orthorhombic phase. Only at the elevated temperature of 135 °C do the interface crystals melt, not into an isotropic liquid, but into an ordered fluid state. This ordered fluid phase we describe as a nematic liquid crystalline phase, which is evidenced by the scattering halo at $2\theta = 19.4°$. Further heating above 180 °C leads to a sudden shift of the scattering halo to lower 2θ values of $2\theta = 18.8°$ (Figure 11b). This phenomenon represents the characteristic transition of the nematic liquid crystalline phase to the isotropic liquid melt state.[56–58]

Our experimental results are consistent with recent molecular dynamic simulations of temperature-dependent conformations of PE molecules adsorbed on CNT surfaces.[59,60] These studies predicted an isotropic-to-nematic liquid crystalline phase transition at the CNT interface at high temperatures. The nematic liquid crystalline phase was shown to induce ordered PE crystals with polymer chains aligning along the CNT axis. It was further pointed

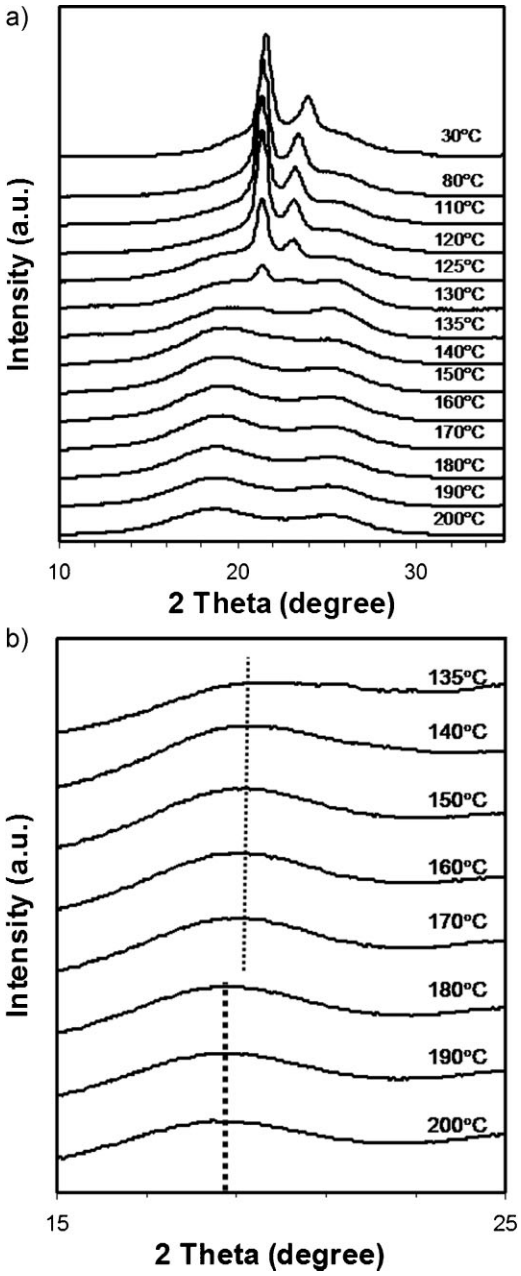

Figure 11. (a) WAXD patterns at various temperatures for the composites prepared from 1 wt.-% solution for 12 h of crystallization, (b) large magnification of (a).

out that the aligned-chain packing of PE crystals in the CNT interface was analogous to the orthorhombic form of PE in the bulk.[60]

Conclusion

We have reported polyethylene oriented crystallization confined in 1 mm long carbon nanotube arrays. Polyethylene solutions have been infiltrated into the nanotube arrays, and the crystallization of the polymer has been controlled. An aligned hybrid shish-kebab nanostructure was seen to form in resultant aligned nanocomposites. The crystallization kinetics demonstrates a heterogeneous nucleation mechanism. As the polymer nanocrystals bind all the aligned nanotubes together rather than fill all the intertube spacing in the nanotube array, the nanotube weight ratio can reach up to ≈80 wt.-%. We have found that the nanotubes act as orientation templates and nucleating agents for the orientation and growth of both orthorhombic and monoclinic crystals of polyethylene, and the orthorhombic crystal phases dominate over the monoclinic ones. Multiple phase transitions were observed and identified to crystal melting in the bulk, crystal melting at the nanotube interface and nematic liquid crystalline transitions at the nanotube interface.

Acknowledgements: We thank *C. Wei* for fruitful discussions. Financial support from the *National Science Foundation* (CMMI-0653337) is gratefully acknowledged.

Received: December 8, 2009; Published online: March 4, 2010; DOI: 10.1002/macp.200900686

Keywords: carbon nanotubes; crystallization; interface; nanocomposites; phase transition

[1] R. H. Baughman, A. A. Zakhidov, W. A. de Heer, *Science* **2002**, *297*, 787.
[2] P. M. Ajayan, J. M. Tour, *Nature* **2007**, *447*, 1066.
[3] J. N. Coleman, U. Khan, Y. K. Gun'ko, *Adv. Mater.* **2006**, *18*, 689.
[4] S. J. Zhang, S. Kumar, *Small* **2008**, *4*, 1270.
[5] S. V. Ahir, Y. Y. Huang, E. M. Terentjev, *Polymer* **2008**, *49*, 3841.
[6] M. B. Bryning, D. E. Milkie, M. F. Islam, J. M. Kikkawa, A. G. Yodh, *Appl. Phys. Lett.* **2005**, *87*, 3.
[7] L. Q. Liu, A. H. Barber, S. Nuriel, H. D. Wagner, *Adv. Funct. Mater.* **2005**, *15*, 975.
[8] R. H. Schmidt, I. A. Kinloch, A. N. Burgess, A. H. Windle, *Langmuir* **2007**, *23*, 5707.
[9] S. S. Rahatekar, K. K. K. Koziol, S. A. Butler, J. A. Elliott, M. S. P. Shaffer, M. R. Mackley, A. H. Windle, *J. Rheol.* **2006**, *50*, 599.
[10] F. M. Du, J. E. Fischer, K. I. Winey, *Phys. Rev. B* **2005**, *72*, 4.
[11] N. Grossiord, J. Loos, L. van Laake, M. Maugey, C. Zakri, C. E. Koning, A. J. Hart, *Adv. Funct. Mater.* **2008**, *18*, 3226.
[12] S. J. V. Frankland, A. Caglar, D. W. Brenner, M. Griebel, *J. Phys. Chem. B* **2002**, *106*, 3046.
[13] K. Liao, S. Li, *Appl. Phys. Lett.* **2001**, *79*, 4225.
[14] H. D. Wagner, *Chem. Phys. Lett.* **2002**, *361*, 57.
[15] L. S. Schadler, S. C. Giannaris, P. M. Ajayan, *Appl. Phys. Lett.* **1998**, *73*, 3842.
[16] S. Zhang, S. Kumar, *Macromol. Rapid Commun.* **2008**, *29*, 557.
[17] M. L. Minus, H. G. Chae, S. Kumar, *Polymer* **2006**, *47*, 3705.
[18] R. Haggenmueller, J. E. Fischer, K. I. Winey, *Macromolecules* **2006**, *39*, 2964.
[19] A. C. Brosse, S. Tence-Girault, P. M. Piccione, L. Leibler, *Polymer* **2008**, *49*, 4680.

[20] K. B. Lu, N. Grossiord, C. E. Koning, H. E. Miltner, B. van Mele, J. Loos, *Macromolecules* **2008**, *41*, 8081.
[21] S. Zhang, M. L. Minus, L. B. Zhu, C. P. Wong, S. Kumar, *Polymer* **2008**, *49*, 1356.
[22] J. N. Coleman, M. Cadek, K. P. Ryan, A. Fonseca, J. B. Nagy, W. J. Blau, M. S. Ferreira, *Polymer* **2006**, *47*, 8556.
[23] J. N. Coleman, M. Cadek, R. Blake, V. Nicolosi, K. P. Ryan, C. Belton, A. Fonseca, J. B. Nagy, Y. K. Gun'ko, W. J. Blau, *Adv. Funct. Mater.* **2004**, *14*, 791.
[24] D. N. Futaba, K. Hata, T. Yamada, T. Hiraoka, Y. Hayamizu, Y. Kakudate, O. Tanaike, H. Hatori, M. Yumura, S. Iijima, *Nat. Mater.* **2006**, *5*, 987.
[25] T. Yamada, T. Namai, K. Hata, D. N. Futaba, K. Mizuno, J. Fan, M. Yudasaka, M. Yumura, S. Iijima, *Nat. Nanotechnol.* **2006**, *1*, 131.
[26] L. B. Zhu, J. W. Xu, F. Xiao, H. J. Jiang, D. W. Hess, C. P. Wong, *Carbon* **2007**, *45*, 344.
[27] S. Zhang, L. Zhu, M. L. Minus, H. G. Chae, S. Jagannathan, C. P. Wong, J. Kowalik, L. B. Roberson, S. Kumar, *J. Mater. Sci.* **2008**, *43*, 4356.
[28] L. Ci, J. Suhr, V. Pushparaj, X. Zhang, P. M. Ajayan, *Nano Lett.* **2008**, *8*, 2762.
[29] N. R. Raravikar, L. S. Schadler, A. Vijayaraghavan, Y. P. Zhao, B. Q. Wei, P. M. Ajayan, *Chem. Mater.* **2005**, *17*, 974.
[30] M. Zhang, K. R. Atkinson, R. H. Baughman, *Science* **2004**, *306*, 1358.
[31] W. Lin, K. S. Moon, C. P. Wong, *Adv. Mater.* **2009**, *21*, 2421.
[32] H. S. Peng, *J. Am. Chem. Soc.* **2008**, *130*, 42.
[33] B. L. Wardle, D. S. Saito, E. J. Garcia, A. J. Hart, R. G. de Villoria, E. A. Verploegen, *Adv. Mater.* **2008**, *20*, 2707.
[34] S. Zhang, L. Zhu, C.-P. Wong, S. Kumar, *Macromol. Rapid Commun.* **2009**, *30*, 1936.
[35] W. Lin, Y. G. Xiu, H. J. Jiang, R. W. Zhang, O. Hildreth, K. S. Moon, C. P. Wong, *J. Am. Chem. Soc.* **2008**, *130*, 9636.
[36] L. B. Zhu, Y. H. Xiu, D. W. Hess, C. P. Wong, *Nano Lett.* **2005**, *5*, 2641.
[37] Z. W. Zhang, Q. Xu, Z. M. Chen, J. Yue, *Macromolecules* **2008**, *41*, 2868.
[38] L. Y. Li, B. Li, M. A. Hood, C. Y. Li, *Polymer* **2009**, *50*, 953.
[39] L. Y. Li, C. Y. Li, C. Y. Ni, *J. Am. Chem. Soc.* **2006**, *128*, 1692.
[40] F. Zhang, H. Zhang, Z. W. Zhang, Z. M. Chen, Q. Xu, *Macromolecules* **2008**, *41*, 4519.
[41] B. Li, L. Li, B. Wang, C. Y. Li, *Nat. Nanotechnol.* **2009**, *4*, 358.
[42] B. S. Hsiao, L. Yang, R. H. Somani, C. A. Avila-Orta, L. Zhu, *Phys. Rev. Lett.* **2005**, *94*, 4.
[43] J. A. Odell, D. T. Grubb, A. Keller, *Polymer* **1978**, *19*, 617.
[44] Z. Bashir, J. A. Odell, A. Keller, *J. Mater. Sci.* **1984**, *19*, 3713.
[45] J. P. Armistead, J. D. Hoffman, *Macromolecules* **2002**, *35*, 3895.
[46] S. J. Zhang, K. K. K. Koziol, I. A. Kinloch, A. H. Windle, *Small* **2008**, *4*, 1217.
[47] H. Uehara, M. Nakae, T. Kanamoto, O. Ohtsu, A. Sano, K. Matsuura, *Polymer* **1998**, *39*, 6127.
[48] L. Fontana, D. Q. Vinh, M. Santoro, S. Scandolo, F. A. Gorelli, R. Bini, M. Hanfland, *Phys. Rev. B* **2007**, *75*, 11.
[49] Q. Yuan, V. G. Rajan, R. D. K. Misra, *Mater. Sci. Eng. B-Adv. Funct. Solid-State Mater.* **2008**, *153*, 88.
[50] M. F. Butler, A. M. Donald, W. Bras, G. R. Mant, G. E. Derbyshire, A. J. Ryan, *Macromolecules* **1995**, *28*, 6383.
[51] X. M. Chen, K. W. Yoon, C. Burger, I. Sics, D. F. Fang, B. S. Hsiao, B. Chu, *Macromolecules* **2005**, *38*, 3883.
[52] M. Kobayashi, H. Tadokoro, *Macromolecules* **1975**, *8*, 897.
[53] E. Hellmuth, B. Wunderli, *J. Appl. Phys.* **1965**, *36*, 3039.
[54] H. Uehara, A. Uehara, M. Kakiage, H. Takahashi, S. Murakami, T. Yamanobe, T. Komoto, *Polymer* **2007**, *48*, 4547.
[55] Y. Takahashi, T. Ishida, M. Furusaka, *J. Polym. Sci. Pt. B-Polym. Phys.* **1988**, *26*, 2267.
[56] R. Q. Zheng, E. Q. Chen, S. Z. D. Cheng, F. C. Xie, D. H. Yan, T. B. He, V. Percec, P. W. Chu, G. Ungar, *Macromolecules* **2000**, *33*, 5159.
[57] Y. Yoon, A. Q. Zhang, R. M. Ho, S. Z. D. Cheng, V. Percec, P. W. Chu, *Macromolecules* **1996**, *29*, 294.
[58] R. Q. Zheng, E. Q. Chen, S. Z. D. Cheng, F. C. Xie, D. H. Yan, T. B. He, V. Percec, P. W. Chu, G. Ungar, *Macromolecules* **1999**, *32*, 3574.
[59] C. Y. Wei, *Nano Lett.* **2006**, *6*, 1627.
[60] C. Y. Wei, *Phys. Rev. B* **2007**, *76*, 10.